

## THE ROLE OF SPARSITY IN INVERSE PROBLEMS FOR NETWORKS WITH NONLINEAR DYNAMICS\*

VICTOR J. BARRANCA<sup>†</sup>, GREGOR KOVACIĆ<sup>‡</sup>, AND DOUGLAS ZHOU<sup>§</sup>

*In memory of Professor David Shenou Cai*

**Abstract.** Sparsity is a fundamental characteristic of numerous biological, social, and technological networks. Network connectivity frequently demonstrates sparsity on multiple spatial scales and network inputs may also possess sparse representations in appropriate domains. In this work, we address the role of sparsity for solving inverse problems in networks with nonlinear and time-evolving dynamics. In the context of pulse-coupled integrate-and-fire networks, we demonstrate that nonlinear network dynamics imparts a compressive coding of both network connectivity and inputs provided they possess a sparse structure. This work thereby formulates an efficient sparsity-based framework for solving several classes of inverse problems in nonlinear network dynamics. Driving the network with a small ensemble of random inputs, we derive a mean-field set of underdetermined linear systems relating the network inputs to the corresponding activity of the nodes via the feed-forward connectivity matrix. In reconstructing the network connections, we utilize compressive sensing theory, which facilitates the recovery of sparse solutions to such underdetermined linear systems. Using the reconstructed connectivity matrix, we are capable of accurately recovering detailed network inputs, which may vary in time, distinct from the random input ensemble. This framework underlines the central role of sparsity in information transmission through network dynamics, providing new insight into the structure-function relationship for high-dimensional networks with nonlinear dynamics. Considering the reconstruction of structural connectivity in large networks is a significant and challenging problem in the study of complex networks, we hypothesize that analogous reconstruction methods taking advantage of sparsity may facilitate key advances in the field.

**Keywords.** Sparsity; neuronal networks; nonlinear dynamics; compressive sensing; network reconstruction; inverse problems.

**AMS subject classifications.** 92C20; 92C42; 82B05; 94A08.

### 1. Introduction

A pervading problem in the study of complex systems is the recovery of network connectivity and network inputs from limited measurements of network dynamics or node interactions. While it is theoretically possible to directly measure the existence of all possible network connections to obtain a full network wiring diagram, often this is quite difficult in practice due to limitations in the spatial resolution of measurement devices or intervention damage when measurements are performed [18, 32, 39, 40, 74, 75]. Nevertheless, in order to fully characterize the relationship between network structure and function, it is crucial to obtain complete network wiring diagrams.

For small neuronal networks, several techniques have been developed to resolve network wiring diagrams, e.g., neuronal staining and electron microscopy, but for larger networks in which more distant connections are included, alternative methodologies are typically necessary [71, 81]. More recently, diffusion tensor imaging (DTI) has been employed to help resolve this issue and tracer injections have also been used to reveal long-range connectivity in the brain, such as inter-areal connections in the macaque cerebral cortex. However, these methods still lack finely resolved spatial resolution

\*Received: October 30, 2018; Accepted (in revised form): May 04, 2019.

<sup>†</sup>Department of Mathematics and Statistics, Swarthmore College, 500 College Avenue, Swarthmore, PA, 19081, USA ([vbarran1@swarthmore.edu](mailto:vbarran1@swarthmore.edu)).

<sup>‡</sup>Mathematical Sciences Department, Rensselaer Polytechnic Institute, 110 8th Street, Troy, NY 12180, USA ([kovacg@rpi.edu](mailto:kovacg@rpi.edu)).

<sup>§</sup>School of Mathematical Sciences, MOE-LSC, and Institute of Natural Sciences, Shanghai Jiao Tong University, Shanghai 200240, China ([zdz@sjtu.edu.cn](mailto:zdz@sjtu.edu.cn)).

[13, 50, 56]. For these reasons, the complete neuronal wiring diagram [73] is known for simple organisms with less than one thousand neurons, such as *Caenorhabditis elegans* [78, 81], but for more complex organisms with many more neurons, resolving such a complete wiring diagram is particularly challenging.

A more indirect yet economical alternative is to instead measure the dynamics of various nodes to infer network connectivity. Such an approach is widely utilized to reveal network structure across diverse systems, including food web [31], ecological [21], regulatory gene interaction [28], and disease-spread networks [47]. Several approaches, both experimental and model-based, have been formulated to infer the functional connectivity or structural connectivity, with varying degrees of success, based on the measurement of individual node dynamics. Such methodologies include the use of cross-correlations in node activity [43], spike-train partial spectral coherence [26], dynamic Bayesian networks [33], and linear Granger causality analysis of a time series of observations [85, 86]. However, for many networks, there are ubiquitous difficulties in accurately inferring network structure from dynamics, such as isolating the impact of multiple time-scale activity, detecting interactions across spatial scales, and addressing indirect node interactions, thereby yielding in general a difficult class of *inverse problems*. Similarly, while in some cases it is possible to recover network inputs from observations of network dynamics [34, 41, 51, 53], when the number of nodes is much smaller than the number of input components, the reconstruction process becomes highly underdetermined.

For large networks with *nonlinear and time-evolving dynamics*, it is particularly crucial to take into account specific network characteristics in formulating an accurate and efficient reconstruction framework. Thus, here we address how it is possible to take advantage of a common structure, namely *sparsity*, generally embedded in both network connectivity and inputs, in optimizing their respective reconstructions. Sparsity is observed on multiple scales in the connectivity of diverse biological, technological, and social networks [1, 4, 44, 58, 80]. For example, both local cortical circuits [58, 59] as well as the retina [37, 38] demonstrate sparse connections between neurons. Similarly, sparse connectivity between cortical and subcortical regions is also well-documented [1, 44]. In this work, we examine how the underlying sparsity of network models with nonlinear state space dynamics facilitates the efficient reconstruction of feed-forward network connectivity as well as detailed network inputs based on the observed network dynamics in response to a relatively small ensemble of inputs.

In formulating our reconstruction framework, we employ a kinetic-theoretic approach as well as *compressive sensing* (CS) theory. Providing a means of efficiently recovering signals which have a sparse representation in a selected domain, CS theory has proven to be a significant advancement in the field of signal processing [24, 25, 29]. Compressive sensing has fostered numerous applications in physics, biology, and image processing [16, 17, 27, 42, 45, 54], enabling the recovery of diverse signals using far fewer measurements than suggested by the Shannon-Nyquist theorem conventionally applied in determining sampling protocols [67].

While applications of CS theory have largely been limited to reconstructing signals from static and linear measurements, we formulate a sparsity-based framework for recovering both the *feed-forward connectivity* and *detailed inputs* for a pulse-coupled integrate-and-fire (I&F) network model with nonlinear node dynamics. Forcing the network with a small ensemble of random inputs, we derive a mean-field set of underdetermined linear systems relating the network inputs to the corresponding activity of the nodes via the feed-forward connectivity matrix. Upon reconstructing the sparse feed-forward connectivity utilizing CS theory, we then use our derived network input-output

relationship to recover realistic network inputs, such as images, videos, or sound waves, which also typically display sparse structure [35].

The results of this work suggest that sparsity plays a key role in facilitating the efficient coding of both network inputs and connectivity through nonlinear network dynamics, providing a new and important link between network structure and function. Considering the observed network response to a relatively small number of inputs facilitates the reconstruction of relatively high dimensional network data, our framework provides efficient solutions to several classes of underdetermined, nonlinear inverse problems.

An outline of the presented results is as follows. First, we describe our feed-forward I&F network model in Section 2.1, and then summarize relevant CS theory in Section 2.2. Next, in Section 2.3, we derive the linear input-output mapping underlying the network dynamics, and then use this mapping as well as CS theory to reconstruct the feed-forward connectivity in Section 3.1. Using the reconstructed connectivity matrix, we also recover network inputs with detailed features and time-evolving dynamics in Section 3.2. In Section 3.3, we analyze the robustness of our methodology by considering the impact of node measurement time, noise, and recurrent connectivity on the reconstruction of feed-forward network connectivity. We conclude by examining future applications and possible ramifications of this work in Section 4.

## 2. Methods

**2.1. Network dynamics and connectivity structure.** The prototypical system we consider is feed-forward and takes the form of a pulse-coupled integrate-and-fire (I&F) network [8, 20, 22, 61, 65, 70, 84]. This network model is comprised of two layers, with I&F dynamics in the output layer, reflecting, for example, the neuronal membrane potential, in response to forcing from the input layer. The dynamics of the  $i^{\text{th}}$  node in the output layer is governed by

$$\tau \frac{dv_i}{dt} = -(v_i - V_R) + \sum_{j=1}^n F_{ij} p_j + \frac{S}{N_R} \sum_{\substack{k=1 \\ k \neq i}}^m R_{ik} \sum_l \delta(t - \tau_{kl}), \quad (2.1)$$

evolving from the reset state  $V_R$  (resting voltage) until reaching threshold state  $V_T$  (firing threshold voltage). At this moment, the node undergoes a spike (firing event), and its state is immediately reset to  $V_R$ . We choose parameters  $V_R = 0$ ,  $V_T = 1$ , and  $\tau = 20$  ms. In addition, we assume  $n$  and  $m$  are the number of input components and output nodes, respectively, with vector  $p = (p_1, \dots, p_n)$  determining the forcing into the output layer. While we choose  $n \gg m$ , such that only a small number of output nodes is necessary to measure relative to the total number of inputs considered, our analysis also holds in the case when  $n \approx m$ .

With regard to network architecture,  $F = (F_{ij})$  is the feed-forward connectivity (adjacency) matrix between the two network layers. We therefore say that the  $i^{\text{th}}$  node in the output layer is post-connected (post-synaptic) to the  $j^{\text{th}}$  input component if  $F_{ij} \neq 0$ . For tractability and generality, we assume that every input component randomly feeds into each output node with equal probability and equal strength,  $f$ . We assume the probability of connection is very low, thereby yielding *sparse* feed-forward connectivity. To quantify the sparsity of connections, we use the notation,  $s(F)$ , denoting the proportion of components in  $F$  with 0 value. Similarly, the density of connections in  $F$ , the proportion of non-zero components in  $F$ , is simply  $1 - s(F)$ . Unless noted otherwise, we choose  $s(F) = 0.999$ , as discussed further in Section 3.1. We simulate the time evolution of this model with an event-driven algorithm, utilizing analytical computations of

node spike times, for a typical time-course of  $t_f = 200$  ms comparable to average human reaction time to stimuli [2, 3]. Later, in Section 3.3, we consider how our framework generalizes to shorter simulation (measurement) durations as well.

Similarly,  $R = (R_{ij})$  is the output layer recurrent connectivity matrix and  $S$  determines the magnitude of the recurrent connections. At the time of the  $l^{\text{th}}$  spike of the  $k^{\text{th}}$  node,  $\tau_{kl}$ , we inject the instantaneous inputs  $(S/N_R)\delta(t - \tau_{kl})$  into all of its neighboring nodes, where  $\delta(\cdot)$  is the Dirac delta function and  $N_R$  is the number of recurrent connections. In the case of a fully feed-forward network,  $R_{ij} = 0$  for all  $i, j$ . It is important to emphasize that the nonlinearity present in this network model is two-fold. First, for each node in the output layer, the instantaneous reset of the node state from threshold state  $V_T$  to reset state  $V_R$  at each spike is nonlinear. Second, upon each of these spikes, the Dirac delta function inputs received by neighboring nodes are also nonlinear.

To reconstruct the feed-forward network connectivity, we inject an ensemble of  $r$  random inputs into the network, corresponding to a set of  $r$  distinct input vectors,  $p^{(1)}, \dots, p^{(r)}$ . In response to each input vector, we measure the average number of spikes observed per unit time, known as the *firing rate*, for each node. Specifically, we measure a vector of firing rate responses of the  $m$  output nodes corresponding to each injected input vector,  $\mu^{(1)}, \dots, \mu^{(r)}$ , where each  $\mu^{(i)}$  is a vector given by  $\mu^{(i)} = (\mu_1^{(i)}, \mu_2^{(i)}, \dots, \mu_m^{(i)})$  for  $1 \leq i \leq r$ , and seek to reconstruct the feed-forward connectivity matrix,  $F$ . We demonstrate that even when the total number of output measurements,  $mr$ , utilized is much less than the number of unknowns in the feed-forward connectivity matrix,  $mn$  (i.e.,  $r < n$ ), the feed-forward network connectivity can still be successfully determined. Moreover, using the reconstructed matrix, we then recover realistic network inputs, *differing from those random inputs injected to infer  $F$* . A schematic model for this reconstruction process is depicted in Figure 2.1.

**2.2. Compressive sensing theory.** To take advantage of both the assumed sparsity of the feed-forward network connectivity and the possible sparsity of the network inputs, we utilize the theory of compressive sensing. For band-limited signals that are sparse in a certain domain, CS theory asserts that, in the sparse domain, the number of non-zero components, rather than the full bandwidth [67], should determine the signal sampling rate for a successful reconstruction [25, 29]. Intuitively, this suggests that for a  $k$ -sparse signal, with  $k$  non-zero components in the sparse domain, only  $O(k)$  measurements should be necessary to obtain the full set of information defining the signal.

In the framework of linear systems analysis, this recovery problem can be expressed in the form

$$Ax = b, \quad (2.2)$$

where  $x$  is the  $n$ -component signal to be recovered and  $b$  is the  $m$ -component measured signal. The sampling scheme is modeled by the  $m \times n$  measurement matrix,  $A$ . Note that each row of  $A$  corresponds to several weighted measurements of signal  $x$ .

Assuming very few samples are used and therefore  $m \ll n$ , Equation (2.2) generally is a highly underdetermined linear system with an infinite number of solutions. Since the sparsest solution to Equation (2.2) best reconciles a small number of signal samples, one intuitive way to choose  $x$  is to directly seek the sparsest solution. However, this approach is computationally expensive and generally not possible to implement in polynomial time, and therefore a more feasible surrogate method is desirable [19]. For sufficiently sparse  $x$  and a broad class of measurement matrices, CS theory shows that such a

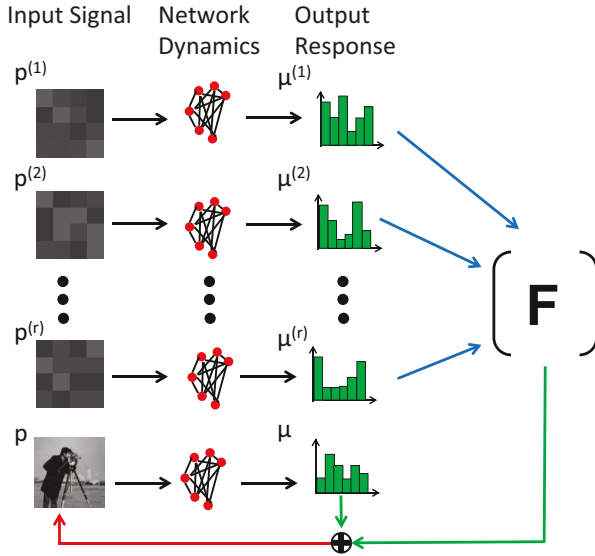


FIG. 2.1. *Schematic procedure for network connectivity reconstruction.* An ensemble of  $r$  network inputs,  $p^{(1)}, \dots, p^{(r)}$ , evokes a set of output node responses,  $\mu^{(1)}, \dots, \mu^{(r)}$ . In the case of the  $i^{\text{th}}$  input vector,  $p^{(i)}$  is an  $n$ -vector and  $\mu^{(i)}$  is an  $m$ -vector such that  $n \gg m$  and  $n \gg r$ . Using the measured responses over the input ensemble, the feed-forward network connectivity matrix,  $F$ , is reconstructed (indicated by blue arrows). Finally, a new network input with detailed structure,  $p$ , can be recovered (indicated by a red arrow) using the corresponding output node response,  $\mu$ , and the reconstructed feed-forward connectivity (indicated by green arrows).

viable surrogate is in fact minimizing  $|x|_{\ell_1} = \sum_{i=1}^n |x_i|$  subject to Equation (2.2) [24]. This  $\ell_1$  optimization problem can be efficiently solved in polynomial time using numerous algorithms, such as the orthogonal matching pursuit (OMP), the least angle regression (LARS), and the least absolute shrinkage and selection operator (LASSO) methods [30, 77].

An important requirement of CS theory is that the sampling methodology demonstrates suitable non-uniformity and incoherence. In particular, if measurement matrix  $A$  exhibits little correlation among its columns and approximately preserves the magnitude of the input signal  $x$ , CS theory demonstrates that with overwhelmingly high probability the solution to Equation (2.2) with the minimal  $\ell_1$  norm will indeed yield a high fidelity reconstruction of the measured signal [5, 25]. This contrasts significantly from sampling requirements corresponding to uniformly-spaced sampling schemes conventional in signal processing theory [67], facilitating the measurement of dominant signal components by using a particularly small total number of samples. In addition, measurement matrices viable for CS are relatively simple to formulate, with a broad class of matrices with independent identically distributed random elements proven to satisfy the CS requirements [24].

**2.3. Network input-output mapping.** In determining the feed-forward network connectivity matrix,  $F$ , we force the network with an ensemble of  $r$  random input vectors. Each input vector is comprised of independent, identically uniformly-distributed integers between 0 (black) and 255 (white), analogous to random gray-scale vectorized images. Thus, the structure of the  $i^{\text{th}}$   $n$ -component input vector,  $p^{(i)}$ , deter-

mines the response of the output nodes, producing a corresponding  $m$ -vector of firing rates  $\mu^{(i)}$ , where  $1 \leq i \leq r$ .

Using only the knowledge of the  $r$  input vectors,  $p^{(1)}, \dots, p^{(r)}$ , and the respective measured firing rates,  $\mu^{(1)}, \dots, \mu^{(r)}$ , we demonstrate that CS theory can be used in reconstructing sparse feed-forward connectivity. However, in order for CS theory to be applicable, it is first necessary to determine an underlying static linear relationship between the network inputs and response analogous to Equation (2.2). Since the network dynamics are both nonlinear and time-dependent, we use the methodology outlined in Refs. [9, 12] to coarse-grain the network dynamics, revealing an input-output mapping for our network model.

In coarse-graining the network model determined by Equation (2.1), for each network input vector, we consider an ensemble of networks differing only in the randomly-determined initial state of the nodes. Corresponding to each such network, there exists a distinct set of output node spiking dynamics and consequently different respective firing rate vectors. Using methods akin to kinetic theory in nonequilibrium statistical mechanics [15, 23, 76], we derive a linear input-output mapping between input vectors and the output node firing rates, which holds for each individual output node and is valid when the firing rates are large,  $\mu_j \gg 1$ , for  $j = 1, 2, \dots, m$ , and the state jump induced by each spike is small in magnitude, such that  $S/N_R \ll 1$ . Details in deriving this input-output mapping are provided in the Appendix. Linearizing this mapping in the high firing rate regime, we obtain the linear input-output relationship

$$Fp = \left( \tau\mu + \frac{e_m}{2} \right) (V_T - V_R) - \frac{S}{N_R} R\mu, \quad (2.3)$$

with  $m$ -vector of ones,  $e_m$ , which holds for each vector of inputs,  $p^{(1)}, \dots, p^{(r)}$ , and corresponding evoked firing rates,  $\mu^{(1)}, \dots, \mu^{(r)}$ . Therefore, we may consider the linear mapping for the complete set of  $r$  input vectors, represented as  $n \times r$  matrix,  $P = (p^{(1)} \dots p^{(r)})$ , where the  $i^{\text{th}}$  column,  $p^{(i)}$ , corresponds to the  $i^{\text{th}}$   $n$ -vector of inputs into the output layer. We remark that in the absence of recurrent connectivity, this mapping reduces to

$$Fp = \left( \tau\mu + \frac{e_m}{2} \right) (V_T - V_R), \quad (2.4)$$

in the high firing-rate dynamical regime.

### 3. Results

**3.1. Reconstruction of feed-forward connectivity.** In reconstructing the connectivity for the two-layer network with dynamics prescribed by Equation (2.1), we reconstruct each row of  $F$  individually using the derived linear mapping across the matrix of input vectors,  $P$ . To recover the strength of all connections received by the  $i^{\text{th}}$  output node, we seek to reconstruct the  $i^{\text{th}}$  row of  $F$ , namely  $F_{i*}$ . We thus consider Equation (2.3) corresponding to the  $i^{\text{th}}$  output node using the full matrix of input vectors,  $P$ , corresponding full matrix of responses,  $U$ , and  $r$ -vector of evoked firing rates for the  $i^{\text{th}}$  output node,  $U_i = (\mu_i^{(1)}, \dots, \mu_i^{(r)})$ . In particular, for the  $i^{\text{th}}$  output node, we analyze the linear system

$$F_{i*}P = \left( \tau U_i + \frac{e_r}{2} \right) (V_T - V_R) - \frac{S}{N_R} (RU)_i, \quad (3.1)$$

for which CS theory is viable in recovering  $F_{i*}$ . Since the feed-forward connectivity matrix,  $F$ , is assumed sparse, as observed for many real-world networks, CS theory is

of utility in efficiently determining the underlying structural connectivity. Moreover, considering that an ensemble of statistically independent random inputs is injected, the matrix of  $r$  inputs,  $P$ , is akin to the measurement matrices feasible for successful CS signal recovery. Applying CS theory to  $F_{i*}$  for  $i=1,\dots,m$ , we obtain a reconstruction of the full feed-forward connectivity matrix,  $F^{\text{recon}}$ , using  $r \ll n$  random input vectors and the measurement of the corresponding response of the  $m$  output nodes. Hence, we reconstruct  $nm$  random connections using only  $rm \ll nm$  measurements. In addition to the computational savings offered by the small number of measurements required for a successful reconstruction, Equation (3.1) is a family of linear systems with multiple right-hand sides, and thus parallel computing could potentially be used to further reduce the computational cost associated with the inverse problem of reconstructing  $F$ .

Note that in reconstructing the network feed-forward connectivity, CS theory motivates the choice of input ensemble structure, implying that utilizing sufficiently uncorrelated input vectors yields an amenable matrix of inputs,  $P$ , which takes the role of the measurement matrix in reconstructing  $F$  via compressive sensing. In this case, the sparsity of  $F$  and the random structure of  $P$  are crucial. As we will discuss in the subsequent section, in recovering a detailed network input,  $p$ , from a single vector of measured output node firing rates,  $\mu$ , a sparse representation of  $p$  and sufficiently random feed-forward network connectivity, as prescribed by  $F$ , are instead significant.

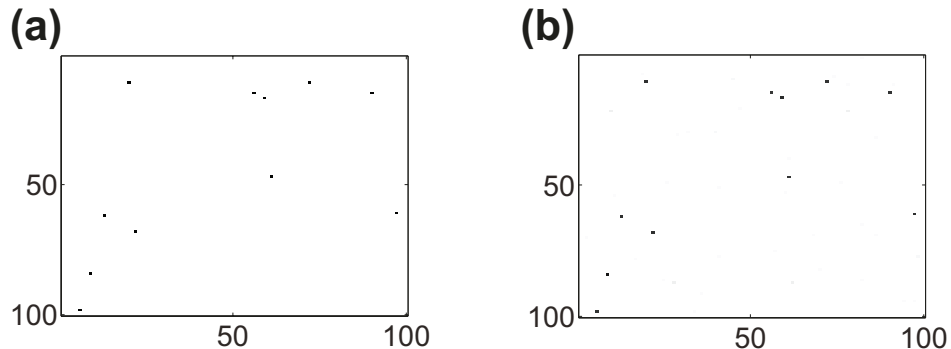


FIG. 3.1. Sample reconstruction of feed-forward network connectivity. (a) Feed-forward connectivity matrix with the first  $100 \times 100$  subset depicted for a network of  $m=1000$  output nodes and  $n=10000$  input components. We plot this subset rather than the full network to make more visible the individual connections marked in black. (b) Reconstructed feed-forward connectivity matrix for the same subset using CS with Equation (3.1) and  $r=1000$  random input vectors. The relative reconstruction error corresponding to the entire  $1000 \times 10000$  connectivity matrix is 0.1263. Using the same methodology with thresholded values for the connection strengths prescribed by function  $\Omega$  in Equation (3.2) with  $\alpha=0.5$ , the relative reconstruction error is further reduced to 0.0453.

We initially focus our analysis on a purely feed-forward network and later consider the impact of recurrent connectivity in Section 3.3. Note that in the absence of recurrent connectivity, we simply assume  $R=0$ . In Figure 3.1, we consider the recovery of the feed-forward connectivity for a network of  $m=1000$  output nodes receiving an input vector of  $n=10000$  input components using  $r=1000$  random input vectors. In Figure 3.1 (a), we depict the network connectivity for the first  $100 \times 100$  subset of the  $1000 \times 10000$  feed-forward connectivity matrix, so as to make each individual connection visible. We recover the feed-forward connectivity matrix for the entire network using CS theory on the linear system given by Equation (3.1) for  $i=1,\dots,m$ , depicting the reconstruction corresponding to the  $100 \times 100$  subset in Figure 3.1 (b). For this subset

of  $F$ , we note that every connection, or lack thereof, is captured exactly.

To quantify the accuracy of the entire feed-forward connectivity matrix reconstruction, we measure the relative reconstruction error,  $\|F - F^{\text{recon}}\|/\|F\|$ , using the Frobenius norm,  $\|F\| = \sqrt{\sum_i \sum_j F_{ij}^2}$ , where  $F^{\text{recon}}$  is the reconstructed feed-forward connectivity matrix. In this particular case, the relative reconstruction error is only 0.1263, yielding close agreement with the original connectivity matrix. If we know a priori the feed-forward connection strength,  $f$ , from assumptions based on experiment [6, 57], then we can further improve the reconstruction quality by thresholding the magnitudes of the entries in the recovered feed-forward connectivity matrix. One viable thresholding procedure is using a thresholding function,  $\Omega$ , such that for each entry of  $m \times n$  matrix,  $F^{\text{recon}}$ ,

$$\Omega_{ij}(F^{\text{recon}}) = \begin{cases} 0, & \text{if } |F_{ij}^{\text{recon}}| < \alpha f, \\ f, & \text{if } |F_{ij}^{\text{recon}}| \geq \alpha f \end{cases}, \quad (3.2)$$

thereby setting each entry of  $F^{\text{recon}}$  with magnitude less than  $\alpha f$  to 0 and all other entries to  $f$ . Using  $\Omega$  with thresholding parameter  $\alpha = 0.5$ , the relative reconstruction error for the network considered in Figure 3.1 is reduced to a value of 0.0453. Moreover, for alternative choices of  $\alpha$ , we observe that similar improvements in reconstruction quality may be garnered.

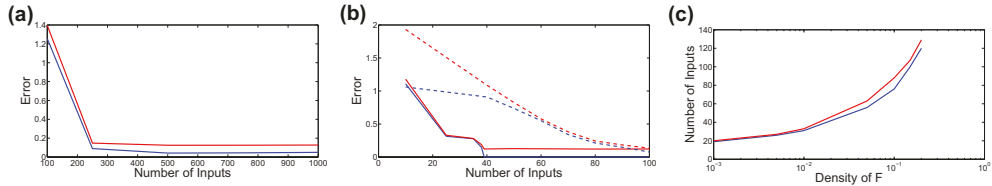


FIG. 3.2. *Relative reconstruction error dependence on the number of input vectors.* (a) Relative reconstruction error for a two-layer network of size  $m=1000$  and  $n=10000$  as a function of the number of input vectors utilized (red lines). The sparsity of the feed-forward connectivity matrix is fixed at  $s(F)=0.999$ . (b) Relative reconstruction error dependence for a smaller two-layer network of size  $m=100$  and  $n=100$ . The sparsity of the feed-forward connectivity matrix is fixed at  $s(F)=0.99$  (solid lines). If additional connections are added to the network in (b), yielding a sparsity  $s(F)=0.9$ , the reconstruction error increases (dashed lines). (c) The number of inputs necessary to achieve an accurate reconstruction of feed-forward connectivity matrix  $F$ , with relative error less than 0.15, as a function of the connection density of  $F$ . The error considered for each choice of connection density is the mean relative reconstruction error over 10 realizations of  $F$ , exhibiting a small average variance of order 0.0001. For (a)-(c), the relative reconstruction error corresponding to thresholded connection strengths, as prescribed by function  $\Omega$  in Equation (3.2) with  $\alpha=0.5$ , is plotted for comparison (blue lines).

In addressing the impact of the input ensemble on the reconstruction framework, we consider in Figure 3.2 (a), the dependence of the relative reconstruction error on the number of random input vectors,  $r$ , used in recovering  $F$  for the same two-layer network of size  $m=1000$  and  $n=10000$ . We observe a rapid decrease in reconstruction error as the number of input vectors increases to approximately 250, with relatively minor improvements in reconstruction quality as the number of input vectors utilized is further increased. In this case, the sparsity of the feed-forward connectivity matrix is fixed at  $s(F)=0.999$ . We note that this particular choice of sparsity corresponds to each input component feeding into approximately one output node, such that little over- or under-sampling of the input vector is utilized.

Likewise, in Figure 3.2 (b), we plot the reconstruction error dependence for a smaller two-layer network of size  $m=100$  and  $n=100$  with sparsity  $s(F)=0.99$ . We observe a similar structure as depicted in Figure 3.2 (a), with a slightly larger proportion of inputs relative to the network size necessary for comparable reconstruction quality. This increase in error is to be expected since the smaller network is less sparse, and therefore successful CS signal recovery should require additional samples. If the sparsity is further decreased to  $s(F)=0.9$  given the same network size, we observe further increases in reconstruction error as also shown in Figure 3.2 (b).

To more generally demonstrate the interplay between connection density and reconstruction accuracy, we plot in Figure 3.2 (c) the number of input vectors necessary for an accurate reconstruction of  $F$  for networks of different connection densities, but with the same size  $m=100$  and  $n=100$ . In each case, a reconstruction is considered sufficiently accurate if it yields a mean error of less than 0.15 over an ensemble of 10 realizations of  $F$  for a given connection density. From Figure 3.2 (c), it is clear that as the density of connections in  $F$  increases (and sparsity of  $F$  decreases), the number of random input vectors required for successful reconstruction of  $F$  increases. Moreover, the rate of increase becomes larger as  $F$  becomes more dense, suggesting that once connections in  $F$  are too dense, CS theory is no longer viable in reconstructing the network connectivity. Nevertheless, such high connection density is not typical in many applications, and thus the density of common structural connectivity matrices should be well within the regime of utility for CS recovery. We also note in Figures 3.2 (a)-(c) that for each choice of connectivity matrix sparsity, thresholding the recovered connection strengths via function  $\Omega$  in Equation (3.2) with  $\alpha=0.5$  results in consistently improved reconstruction quality. Thus, assuming the expected connection strength may be estimated experimentally, such thresholding is quite useful in rendering improved estimation of  $F$  for little additional computational cost. Even without thresholding, the accuracy of each reconstructed  $F$  across realistic connection densities is especially high considering such a small number of measurements is typically utilized.

**3.2. Network input recovery.** Upon reconstruction of the feed-forward connectivity matrix, we demonstrate that it is possible to subsequently recover detailed network inputs using CS theory with the input-output mapping (2.4) and the reconstructed feed-forward connectivity matrix. We show that even for natural scene inputs, differing significantly in structure from the random input vectors used to reconstruct  $F$ , high fidelity recovery of inputs signals is achievable even when the input vectors have significantly more components than the number of output nodes.

If the input vector is not sparse in its initial representation, it is first necessary to determine an appropriate sparsifying transform before utilization of CS theory. To reconstruct a novel two-dimensional input image with vectorization  $p=(p_1, \dots, p_n)$ , we use the two-dimensional discrete cosine transform (2D-DCT) to sparsify the signal. We remark that for one-dimensional inputs, analogous to sound waves, we need only consider the one-dimensional discrete cosine transform (1D-DCT) using the same methodology described in this section.

The  $\sqrt{n} \times \sqrt{n}$  1D-DCT,  $D$ , is defined to have entries  $D_{ij} = (D^{-1})_{ij}^T = \omega(i) \cos\left(\frac{(i-1)(2j-1)\pi}{2\sqrt{n}}\right)$ ,  $\omega(1) = (1/n)^{1/4}$ , and  $\omega(i \neq 1) = (4/n)^{1/4}$ . The 2D-DCT of an image with vectorization  $p$  is  $(D \otimes D)p$ , where  $\otimes$  denotes the  $n \times n$  Kronecker product

defined such that

$$D \otimes D = \begin{bmatrix} D_{11}D & \cdots & D_{1\sqrt{n}}D \\ \vdots & \ddots & \vdots \\ D_{\sqrt{n}1}D & \cdots & D_{\sqrt{n}\sqrt{n}}D \end{bmatrix}.$$

Given a vectorized input image, to recover the vectorization of its 2D-DCT,  $\hat{p}$ , we rewrite Equation (2.3) with respect to the 2D-DCT and reconstructed feed-forward connectivity matrix,  $F^{\text{recon}}$ , as

$$\sum_{j=1}^n F_{ij}^{\text{recon}} (D \otimes D)_{ij}^{-1} \hat{p}_j = \left( \tau \mu_i + \frac{e_m}{2} \right) (V_T - V_R) - \frac{S}{N_R} (RU)_i. \quad (3.3)$$

Considering  $\hat{p}$  is sparse, upon measuring the output node firing rates,  $\mu = (\mu_1, \dots, \mu_m)$ , we then invoke CS theory in selecting the solution to Equation (3.3) that minimizes the  $\ell_1$  norm,  $\sum_{j=1}^n |\hat{p}_j|$  [25, 29]. Finally, we invert the 2D-DCT and the vectorization to yield a recovery of the original input image.

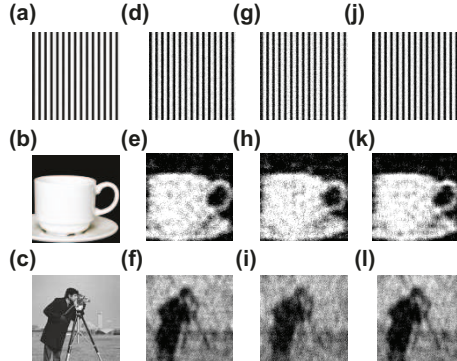


FIG. 3.3. *Input image recoveries using CS theory and the reconstructed feed-forward connectivity from evoked nonlinear network dynamics.* (a)-(c): Input images of size  $100 \times 100$  pixels. (d)-(f): CS recoveries using network dynamics and the exact feed-forward connectivity matrix,  $F$ . (g)-(i): CS recoveries using network dynamics and reconstructed connectivity matrix,  $F^{\text{recon}}$ , without thresholding connection strengths. (j)-(l): CS recoveries using network dynamics and reconstructed connectivity matrix,  $\Omega(F^{\text{recon}})$ , utilizing thresholding function  $\Omega$  in Equation (3.2) with  $\alpha=0.5$ . The relative recovery errors for (d)-(f) are 0.0895, 0.2634, and 0.2345, respectively. The relative recovery errors for (g)-(i) are 0.1171, 0.2844, and 0.2708, respectively. The relative recovery errors for (j)-(l) are 0.0816, 0.2569, and 0.2341, respectively. Each connectivity matrix was reconstructed using an ensemble of  $r=1000$  random input vectors. For each image, the corresponding two-layer network size is  $m=1000$  and  $n=10000$ , with a sparsity of feed-forward connections  $s(F)=0.999$ .

In Figure (3.3), we analyze three input images of varying complexity, depicted in Figure (3.3) (a)-(c), and various CS reconstructions for a two-layer network of size  $m=1000$  and  $n=10000$ . We display in Figure (3.3) (g)-(i) the corresponding recovered images using network dynamics and the reconstructed feed-forward connectivity matrix,  $F^{\text{recon}}$ , obtained previously using  $r=1000$  random input vectors. Likewise, in Figure (3.3) (j)-(l), we alternatively recover these images using thresholded connectivity matrix,  $\Omega(F^{\text{recon}})$ . For the simpler stripe and teacup images, we observe comparably accurate image recovery with both reconstructed connectivity matrices. For the more complex cameraman image, the thresholded connectivity matrix yields a more visually

noticeable improvement in recovery accuracy, with both yielding recognizable recoveries. For comparison, we also display analogous recoveries using the true feed-forward connectivity matrix,  $F$ , in Figure (3.3) (d)-(f). For each image, the recovery quality using  $F$  is nearly identical to the quality obtained via the reconstructed connectivity matrix using thresholding. Thus, the reconstructed thresholded connectivity matrix,  $\Omega(F^{\text{recon}})$ , appears useful as a viable surrogate for the actual connectivity matrix given by  $F$  without noticeably degrading the input image recovery.

It is important to note that improved network input recovery is possible for input signals containing more components, such as higher resolution images that possess a larger number of pixels [10]. While additional higher-frequency components are introduced when the resolution of an image is improved, the amplitude distribution of the dominant frequency components is often nearly indistinguishable from the lower resolution image counterpart. As the input vector size is increased, maintaining a constant ratio of output nodes to input components effectively requires increasing the number of output nodes while only minorly altering the dominant frequency components of the input, and these additional node response measurements will generally increase the accuracy of input recovery as the dominant frequency-components become better resolved.

We emphasize that each of these recovered images was not in the ensemble of random input vectors used to reconstruct  $F$ . Nevertheless, as a result of two-fold sparsity in the network connectivity and inputs, it is possible to successfully determine both the feed-forward network connectivity and also detailed input vectors driving the network dynamics using only limited measurements of the nonlinear activity of the output nodes, thereby providing a framework for solving several classes of underdetermined inverse problems for networks with nonlinear dynamics.

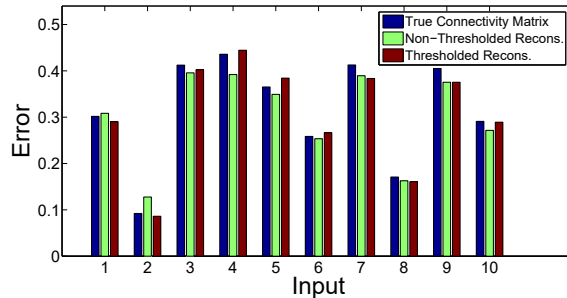


FIG. 3.4. Recovery of an ensemble of input images. Relative recovery errors corresponding to compressive sensing of network dynamics for an ensemble of 10 randomly selected natural images from the University of Southern California Signal and Image Processing Institute miscellaneous volume of images (<http://sipi.usc.edu/database/database.php?volume=misc>) are depicted. The plotted errors correspond to input recovery via the true feed-forward connectivity matrix,  $F$  (blue), the reconstructed feed-forward connectivity matrix,  $F^{\text{recon}}$  (green), and the thresholded reconstructed connectivity matrix  $\Omega(F^{\text{recon}})$  using thresholding function  $\Omega$  in Equation (3.2) with  $\alpha=0.5$  (red). For each image, the corresponding two-layer network size is  $m=1000$  and  $n=10000$ , with a sparsity of feed-forward connectivity  $s(F)=0.999$ . The mean relative recovery errors using  $F$ ,  $F^{\text{recon}}$ , and  $\Omega(F^{\text{recon}})$  are 0.3146, 0.3026, and 0.3083, respectively.

To examine the robustness of these results, we recover an ensemble of 10 additional natural image inputs using the same two-layer network of size  $m=1000$  and  $n=10000$ . For each image, we compare recoveries using the true feed-forward connectivity matrix,  $F$ , the reconstructed feed-forward connectivity matrix,  $F^{\text{recon}}$ , and the thresholded re-

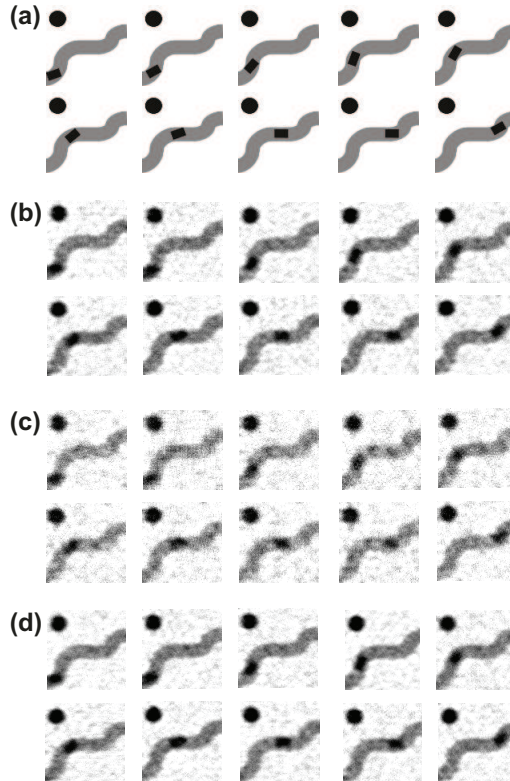


FIG. 3.5. Recovery of video input. (a) Image frames of size  $100 \times 100$  pixels, composing a 10 frame video. (b) CS recoveries using network dynamics and the exact feed-forward connectivity matrix,  $F$ . (c) CS recoveries using network dynamics and reconstructed connectivity matrix,  $F^{\text{recon}}$ , without thresholding connection strengths. (d) CS recoveries using network dynamics and reconstructed connectivity matrix,  $\Omega(F^{\text{recon}})$ , utilizing thresholding function  $\Omega$  in Equation (3.2) with  $\alpha = 0.5$ . Image frames are injected into the network for a duration of 200 ms each. The same two-layer network and  $F^{\text{recon}}$  as in Figure 3.3 (a) are utilized. The average relative recovery errors are 0.1260, 0.1766, and 0.1239, for videos (b)-(d), respectively.

constructed connectivity matrix  $\Omega(F^{\text{recon}})$  in Figure 3.4. In each case, we observe similar image recovery results across the entire ensemble of images, suggesting close agreement in transmitted input information using both the true and reconstructed network connections. Considering that each feed-forward connectivity utilized yields acceptable recoveries across a diverse set of inputs, we also conclude that input information is generally well-preserved through the nonlinear network dynamics.

We similarly observe that time-varying inputs may also be successfully recovered using an analogous framework following the reconstruction of the feed-forward connectivity. We consider inputs in the form of videos composed of a sequence of image frames which change every 200 ms. For the duration of each image frame injection, we measure the corresponding set of output node firing rates. For each set of firing rates, we then solve the corresponding CS problem in Equation (3.3) to recover the respective image frames. After considering the complete set of image frame CS recovery problems, we obtain the recovered full video.

In Figure 3.5, we consider the CS recovery of a 10 image frame video of a car

navigating through a sunlit road using the same two-layer network and reconstructed connectivity as in Figure 3.3 (a). We depict in Figure 3.5 (b)-(d) the CS recoveries using  $F$ ,  $F^{\text{recon}}$ , and  $\Omega(F^{\text{recon}})$ , respectively. For each video, we observe a very recognizable recovery, with especially high accuracy in the cases of  $F$  and  $\Omega(F^{\text{recon}})$ . While the observation time for each frame is comparable to human reaction time [2, 3], we note that we may further decrease the injection time and still yield fairly accurate recoveries, as we will further discuss in Section 3.3.

**3.3. Robustness and recurrent connectivity.** While thus far we have analyzed the reconstruction of network connections for a feed-forward network model through measurement of output node firing rates over a fixed period of time, we now similarly consider how our analysis generalizes to several alternative scenarios. First, we consider the dependence of reconstruction error on the amount of time over which firing rates are measured, and then we take into account the presence of noise in the measurement of output node dynamics. Finally, we examine how the reconstruction of the feed-forward connectivity is impacted by the presence of additional recurrent connectivity among output nodes.

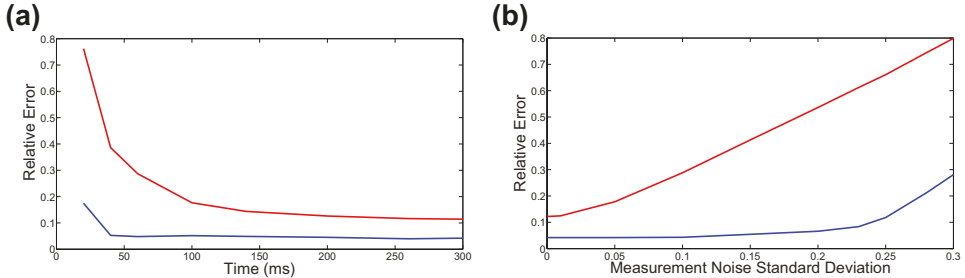


FIG. 3.6. *Robustness of the feed-forward network connectivity reconstruction.* (a) Dependence of the relative reconstruction error for the reconstructed feed-forward connectivity matrix,  $F^{\text{recon}}$ , on the length of time over which firing rates are measured (red line). (b) Relative reconstruction error for  $F^{\text{recon}}$  given noisy firing rate measurements (red line), which are perturbed by independent, identically distributed zero-mean Gaussian random variables with standard deviation  $\sigma$ . The same two-layer network as in Figure 3.3 (a) is utilized. For both (a) and (b), the relative reconstruction error corresponding to the thresholded reconstructed connectivity matrix,  $\Omega(F^{\text{recon}})$ , as prescribed by thresholding function  $\Omega$  in Equation (3.2) with  $\alpha=0.5$ , is plotted in blue for comparison.

For the same  $m=1000$  and  $n=10000$  two-layer network considered previously in Section 2.3, we plot in Figure 3.6 (a) the feed-forward connectivity matrix relative reconstruction error as we vary the length of time over which output node activity is measured. We observe a rapid initial decrease in error as the measurement time is increased with only minor decreases in error upon further increasing measurement time. In addition, using thresholded connection strengths improves the reconstruction accuracy across all measurement times and also results in a more rapid initial decrease in error. By recording firing rates over a period of time as short as 50 ms, nearly optimal reconstructions are achieved in the case of the thresholded feed-forward connectivity matrix.

In experimental settings, the measurement of node activity may vary depending on the recording technique utilized and may also be subject to a small amount of noise [55, 64, 83]. Therefore, we examine the impact of imperfect firing rate recordings on the feed-forward connectivity reconstruction. To each recorded firing rate, we add

noise in the form of an independent, identically distributed Gaussian random variable with zero mean and standard deviation  $\sigma$ . We choose zero mean random variables under the assumption that the distortion due to noise has no general upward or downward bias in firing rate recording. In Figure 3.6 (b), we plot the relative reconstruction error for  $F$  as a function of  $\sigma$ . For sufficiently large  $\sigma$ , we observe an approximately linear increase in error. For low  $\sigma$ , we instead note relatively little increase in error with  $\sigma$ , which holds for a particularly large range of standard deviations in the case of thresholded connection strengths. In the case of  $\Omega(F^{\text{recon}})$ , it is not until  $\sigma \approx 0.25$  that there is any notable impact of noise on the reconstruction, which is a particularly high noise strength since the total input into each output node is  $\mathcal{O}(1)$ . Thus, we conclude that the connectivity reconstruction framework is indeed quite robust to moderately noisy measurements which may arise from experiment.

Finally, we determine if accurate reconstruction of the feed-forward connectivity is achievable in the presence of stronger recurrent interactions. Initially, we assume full knowledge of the recurrent connectivity matrix,  $R$ , but we later consider how the results may change when  $R$  is unknown. We plot the relative reconstruction error dependence on the number of input vectors used in Figure 3.7 (a) for a two-layer network of size  $m = 1000$  and  $n = 10000$  given recurrent connectivity with sparsity  $s(R) = 0.95$  and recurrent connection strength  $S = 1$ . We observe only a minor degradation in reconstruction quality as compared to the network with purely feed-forward connectivity, implying that, as long as the recurrent connections are not too strong, feed-forward connectivity can still be well reconstructed through measurement of the output node dynamics.

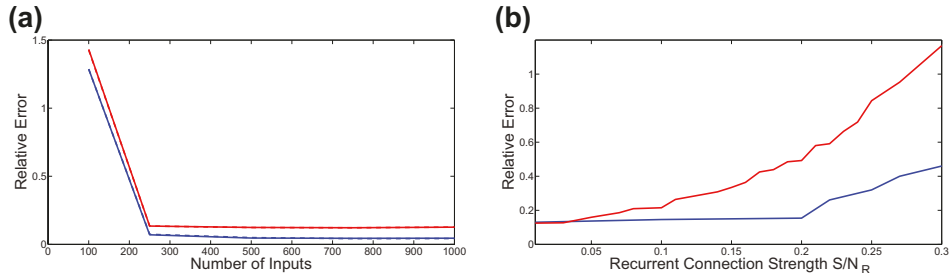


FIG. 3.7. *Impact of recurrent connectivity on feed-forward connectivity reconstruction.* (a) Feed-forward connectivity relative reconstruction error dependence on the number of input vectors utilized for a network with both feed-forward connectivity and recurrent connectivity between the output nodes (red lines), as prescribed by model (2.1). The sparsity of the recurrent connectivity is  $s(R) = 0.95$  and the recurrent connection strength is  $S = 1$ . The corresponding two-layer network size is  $m = 1000$  and  $n = 10000$ , with a sparsity of feed-forward connectivity  $s(F) = 0.999$ . Plotted in solid lines is the relative reconstruction error assuming the recurrent connectivity matrix is known. Plotted in dashed lines is the relative reconstruction error assuming there is no recurrent connectivity while recurrent connectivity is in fact present. (b) Relative reconstruction error dependence on recurrent connectivity strength,  $S/N_R$ , using the same two-layer network parameters as in Figure 3.2 (b) and  $r = 33$  inputs. For both (a) and (b), the relative reconstruction error corresponding to the thresholded reconstructed connectivity matrix,  $\Omega(F^{\text{recon}})$ , as prescribed by thresholding function  $\Omega$  in Equation (3.2) with  $\alpha = 0.5$ , is plotted for comparison (blue lines).

For the same network structure, we alternatively can assume no knowledge of the present recurrent connectivity, therefore not considering  $R$  in reconstructing  $F$ . In this case, we use Equation (3.1) with  $R = 0$  to reconstruct the feed-forward connectivity even though the model still evolves with recurrent interactions according to the dynamics of Equation (2.1). With this methodology, which assumes non-complete knowledge of the

true network structure, we observe nearly identical reconstruction quality for the feed-forward connectivity matrix. Similar trends also hold for networks with moderately strong recurrent connectivity. In Figure 3.7 (b), we plot the relative reconstruction error for  $F$  as a function of the strength of recurrent interactions,  $S/N_R$ . For moderate strengths, we observe only small increases in reconstruction error, with more pronounced escalation in error for sufficiently large  $S$ . Using the thresholded reconstructed feed-forward connectivity matrix, the strengths must be increased up to  $S/N_R \approx 0.2$  before there are any noticeable degradations in the reconstruction, with slow linear growth in error for yet larger recurrent connection strengths. Hence, even when measurement of the recurrent connectivity is not possible, high-fidelity reconstruction of feed-forward connectivity is still achievable. We also verified that the detailed input recoveries are nearly identical to the corresponding recoveries in the case of the completely feed-forward network, and thus we conclude that input information is also well-preserved through the nonlinear network dynamics even with no a priori knowledge of both the feed-forward and recurrent connectivity.

#### 4. Discussion

In this work, we underlined the central role of sparsity in reconstructing network data based on limited measurements of network dynamics. We demonstrated that sparse feed-forward connectivity can be reconstructed from the measurement of the nonlinear dynamics of output nodes in response to a relatively small ensemble of random input vectors, and showed further that the reconstructed connectivity matrix can then be used to recover detailed network inputs based on the evoked output node dynamics. Although previous studies have used learning to make similar recoveries of network inputs possible for static or linear dynamical systems [36, 49], our analysis demonstrates that even for networks with nonlinear state space dynamics, the recovery of both network connections and inputs is achievable by considering only a set of underlying linear systems linking the network input to the measured output response. Additionally, a distinguishing feature of our theory is that the subsequently recovered inputs are not members of the input ensemble and may be realistic natural scenes which change with time. We thereby formulate an efficient solution methodology for a large class of underdetermined inverse problems based only on restricted measurements of nonlinear network dynamics and sparse network connectivity structure.

Our theoretical analysis suggests an important parallel with the development of human vision following infancy, when the observation of a sufficient number of natural scenes results in fully accurate visual acuity with minimal further improvements over time [52, 69]. Similarly, our framework initially suggests a rapid increase in image recovery fidelity as new images are processed, with improvements leveling off once a sufficient number of inputs is injected. Since both the connectivity and inputs into the model network may be inferred within biologically plausible time-scales, we hypothesize that neuronal networks in the brain may use similar techniques in fine-tuning sensory processing and enabling perception in general.

While we have derived a framework for reconstructing sparse feed-forward network connectivity in the context of an integrate-and-fire network model, similar techniques may be ubiquitous in alternative applications. Experimentally, it may be feasible to similarly study feed-forward neuronal connectivity through random stimulation of upstream neurons, and measuring the response of the downstream network of interest. Once an underlying input-output relationship is determined, such as through nonlinear systems analysis as in Refs. [68, 79, 82], it should then be possible to determine the feed-forward connectivity using a small set of random inputs. In other model-based applications,

coarse-graining may yield analogous input-output mappings for additional types of networks with sparse connectivity, allowing for efficient inference of the underlying network connectivity or inputs.

Similar feed-forward network architectures are quite common in engineering and learning applications [46, 66, 72], and it is likely that the outlined framework may be useful in determining neural network feed-forward connectivity following sufficient training. In addition, for feed-forward networks with additional layers, similar techniques potentially apply in efficiently reconstructing the connectivity among the full set of layers. It would be especially useful to determine if compressive sensing techniques may also facilitate the reconstruction of sparse recurrent connectivity, but this would require revealing a novel alternative network structure or dynamical regime necessary for successful reconstruction.

While we make the assumption of sparse and random feed-forward connectivity in our model, realistic networks may have alternative connectivity structures, displaying, for example, localization [62, 63], inhibitory interactions [7], and small-world structure [14, 48, 60]. Considering previous work has demonstrated that localized random connectivity can be used to successfully recover sparse inputs via compressive sensing of network dynamics [9–11], we expect that alternative types of sparse connectivity are amenable to our framework. Efficiently reconstructing both the connectivity and realistic inputs for networks with nonlinear dynamics, we expect this work to be useful in determining the structure-function relationship for a broad class of networks with sparse connectivity or sparse inputs.

**Appendix.** In deriving the linear input-output mapping given by Equation (2.3), we consider a statistical ensemble of networks differing only in the initial state of nodes,  $v_j(t=0)$ , and their resultant time evolution for  $j = 1, \dots, m$ . As a result, for each network realization in the ensemble, the  $j^{\text{th}}$  node is forced by a new independent spike train of pulses transmitted by neighboring nodes in addition to a constant external input,  $(Fp)_j$ . We assume the network possesses the same connectivity structure, prescribed by  $F$  and  $R$ , in each realization.

Over the set of all realizations considered, we analyze the configuration probability,  $P_j(v, dv, t)$ , of the  $j^{\text{th}}$  node having state variable inside the infinitesimally small interval  $(v, v + dv)$  at a specific time,  $t$ . To study this probability, we introduce an associated probability density function,  $\rho_j(v, t)$ , such that the configuration probability we investigate is  $\rho_j(v, t)dv$ . In determining the dynamics of  $P_j(v, dv, t)$ , we consider its evolution over the small time interval  $(t, t + dt)$ .

There are two types of modifications that the configuration probability can undergo, specifically (a) smooth and (b) instantaneous changes. When the  $j^{\text{th}}$  node receives no spikes and is therefore continuously evolving, its configuration probability will adjust according to Equation (2.1) via forcing from feed-forward input  $(Fp)_j$ . At the instant the  $j^{\text{th}}$  node receives a spike from one of its neighbors, its state will immediately change, thereby instantaneously altering its associated configuration probability. We group the smooth parts of Equation (2.1) into function  $\phi(v_j)$  and express the dynamics of the  $j^{\text{th}}$  node in form

$$\frac{dv_j}{dt} = \phi(v_j) + \frac{S}{\tau N_R} \sum_{\substack{k=1 \\ k \neq j}}^m R_{jk} \sum_l \delta(t - \tau_{kl}),$$

where  $\phi(v_j) = \frac{-(v_j - V_R)}{\tau} + \frac{(Fp)_j}{\tau}$ . Hence, for the  $j^{\text{th}}$  node, (a) the smooth change will be

$$[\phi(v)\rho_j(v, t) - \phi(v + dv)\rho_j(v + dv, t)]dt$$

and (b) the instantaneous change will be

$$\sum_{i \neq j} \mu_i \left[ \rho_j \left( v - \frac{SR_{ji}}{\tau N_R}, t \right) - \rho_j(v, t) \right] dv dt.$$

In total, the associated configuration probability evolves according to

$$\begin{aligned} & [\rho_j(v, t + dt) - \rho_j(v, t)] dv \\ &= [\phi(v) \rho_j(v, t) - \phi(v + dv) \rho_j(v + dv, t)] dt + \sum_{i \neq j} \mu_i \left[ \rho_j \left( v - \frac{SR_{ji}}{\tau N_R}, t \right) - \rho_j(v, t) \right] dv dt. \end{aligned}$$

Taylor expanding to  $\mathcal{O}(dv)$  and dividing by the product of differentials  $dv dt$  in the limit as  $dv \rightarrow 0$  and  $dt \rightarrow 0$ , we derive the Boltzmann equation for  $\rho_j(v, t)$

$$\frac{\partial \rho_j}{\partial t} = -\frac{\partial}{\partial v} (\phi \rho_j) + \sum_{i \neq j} \mu_i \left[ \rho_j \left( v - \frac{SR_{ji}}{\tau N_R}, t \right) - \rho_j(v, t) \right],$$

valid for  $V_R < v < V_T$ . Assuming the changes in the state variable at spikes are small, we Taylor expand in  $\frac{SR_{ji}}{\tau N_R}$  to  $\mathcal{O}\left(\left(\frac{SR_{ji}}{\tau N_R}\right)^2\right)$ , obtaining the Fokker-Planck equation

$$\frac{\partial \rho_j}{\partial t} = \frac{\partial}{\partial v} \left( \frac{(v - V_R)}{\tau} \rho_j - g_j \rho_j + \frac{\sigma_j^2}{2} \frac{\partial \rho_j}{\partial v} \right),$$

where

$$g_j = \sum_{i \neq j} \mu_i \frac{SR_{ji}}{\tau N_R} + \frac{(Fp)_j}{\tau}$$

is the mean forcing for the  $j^{\text{th}}$  node and

$$\sigma_j^2 = \sum_{i \neq j} \left( \frac{SR_{ji}}{\tau N_R} \right)^2 \mu_i$$

is the variance in the input fluctuations of the  $j^{\text{th}}$  node.

The Fokker-Planck equation may be expressed in terms of the probability flux of the state variable,  $-J_j$ , in the form of the conservation equation

$$\frac{\partial \rho_j}{\partial t} + \frac{\partial J_j}{\partial x} = 0.$$

Since upon reaching  $V_T$ , the state variable is instantaneously reset to  $V_R$ , the state variable flux at  $v = V_T$  and  $v = V_R$  must be equal. Considering that the  $j^{\text{th}}$  node has a firing rate of  $\mu_j$ , the equality of flux across the boundary yields necessary boundary conditions  $J_j(v = V_T) = J_j(v = V_R) = \mu_j$ .

For the Fokker-Planck equation to be analytically tractable, we consider network dynamics in the *mean-driven* operating regime, such that the variance in input fluctuations is negligible. Thus,  $\sigma_j^2 \rightarrow 0$ , and we obtain the reduced partial differential equation

$$\frac{\partial \rho_j}{\partial t} = \frac{\partial}{\partial v} \left( \frac{(v - V_R)}{\tau} \rho_j - g_j \rho_j \right).$$

Assuming the firing rates and corresponding configuration probability density function are stationary given the dynamics are mean-driven, namely  $\frac{\partial \rho_j}{\partial t} = 0$ , the Fokker-Planck equation is reduced to the ordinary differential equation

$$\frac{\partial}{\partial v} \left( \frac{(v - V_R)}{\tau} \rho_j - g_j \rho_j \right) = -\frac{\partial J_j}{\partial v} = 0,$$

which can be solved analytically for  $\rho_j$ , where

$$\rho_j = \frac{\tau \mu_j}{\tau g_j - (v - V_R)}.$$

Since  $\rho_j$  is a probability density function over  $V_R \leq v \leq V_T$ , it is required to satisfy the normalization condition  $\int_{V_R}^{V_T} \rho_j(v) dv = 1$ , and therefore we obtain the implicit algebraic expression relating the input and firing rate response for the  $j^{\text{th}}$  node

$$1 = (\tau \mu_j) \ln \left( \frac{\tau g_j}{\tau g_j - (V_T - V_R)} \right).$$

The forcing from the feed-forward input,  $(Fp)_j$ , can then be expressed explicitly as

$$(Fp)_j = \frac{(V_T - V_R)}{1 - \exp \left( \frac{-1}{\tau \mu_j} \right)} - \frac{S}{N_R} (R\mu)_j.$$

Assuming the feed-forward input into each node is relatively large, as naturally required in the mean-driven operating regime, the number of firing events for each node within time scale  $\tau$  is  $\mathcal{O}(1)$ . Under this assumption, we Taylor expand about small  $\frac{1}{\tau \mu_j}$  to  $\mathcal{O} \left( \frac{1}{\tau \mu_j} \right)$  and obtain

$$(Fp)_j = \tau \mu_j (V_T - V_R) + \frac{(V_T - V_R)}{2} - \frac{S}{N_R} (R\mu)_j.$$

Enforcing the above for output nodes  $j = 1, \dots, m$  finally yields the linear input-output mapping

$$Fp = \left( \tau \mu + \frac{e_m}{2} \right) (V_T - V_R) - \frac{S}{N_R} R\mu.$$

**Acknowledgments.** This work is supported by NSF DMS-1812478 (V.J.B.), a Swarthmore Faculty Research Support Grant (V.J.B.), NSFC-11671259, NSFC-11722107, NSFC-91630208, SJTU-UM Collaborative Research Program (D.Z.), and the Student Innovation Center at Shanghai Jiao Tong University.

## REFERENCES

- [1] S. Achard and E. Bullmore, *Efficiency and cost of economical brain functional networks*, PLoS Comput. Biol., **3**(2):e17, 2007. 1
- [2] K. Amano, N. Goda, S. Nishida, Y. Ejima, T. Takeda, and Y. Ohtani, *Estimation of the timing of human visual perception from magnetoencephalography*, J. Neurosci., **26**(15):3981–3991, 2006. 2.1, 3.2

- [3] S. Ando, Y. Yamada, and M. Kokubu, *Reaction time to peripheral visual stimuli during exercise under hypoxia*, *J. Appl. Physiol.*, **108**(5):1210–1216, 2010. 2.1, 3.2
- [4] A.L. Barabasi and R. Albert, *Emergence of scaling in random networks*, *Science*, **286**(5439):509–512, 1999. 1
- [5] R. Baraniuk, *Compressive sensing*, *IEEE Signal Process. Mag.*, **118**–120, 2007. 2.2
- [6] B. Barbour, N. Brunel, V. Hakim, and J.P. Nadal, *What can we learn from synaptic weight distributions?* *Trends Neurosci.*, **30**(12):622–629, 2007. 3.1
- [7] V.J. Barranca, H. Huang, and S. Li, *The impact of spike-frequency adaptation on balanced network dynamics*, *Cogn. Neurodyn.*, **13**(1):105–120, 2019. 4
- [8] V.J. Barranca, D.C. Johnson, J.L. Moyher, J.P. Sauppe, M.S. Shkarayev, G. Kovacić, and D. Cai, *Dynamics of the exponential integrate-and-fire model with slow currents and adaptation*, *J. Comput. Neurosci.*, **37**(1):161–180, 2014. 2.1
- [9] V.J. Barranca, G. Kovacić, D. Zhou, and D. Cai, *Sparsity and compressed coding in sensory systems*, *PLoS Comput. Biol.*, **10**(8):e1003793, 2014. 2.3, 4
- [10] V.J. Barranca, G. Kovacić, D. Zhou, and D. Cai, *Improved compressive sensing of natural scenes using localized random sampling*, *Sci. Rep.*, **6**:31976, 2016. 3.2, 4
- [11] V.J. Barranca and X.G. Zhu, *A computational study of the role of spatial receptive field structure in processing natural and non-natural scenes*, *J. Theor. Biol.*, **454**:268–277, 2018. 4
- [12] V.J. Barranca, G. Kovacić, D. Zhou, and D. Cai, *Efficient image processing via compressive sensing of integrate-and-fire neuronal network dynamics*, *Neurocomputing*, **171**:1313–1322, 2016. 2.3
- [13] P.J. Basser, J. Mattiello, and D. LeBihan, *MR diffusion tensor spectroscopy and imaging*, *Biophys. J.*, **66**(1):259–267, 1994. 1
- [14] D.S. Bassett and E. Bullmore, *Small-world brain networks*, *Neuroscientist*, **12**(6):512–523, 2006. 4
- [15] R. Ben-Yishai, R. Bar-Or, and H. Sompolinsky, *Theory of orientation tuning in the visual cortex*, *Proc. Natl. Acad. Sci. USA*, **92**:3844–3848, 1995. 2.3
- [16] C.R. Berger, Z. Wang, J. Huang, and S. Zhou, *Application of compressive sensing to sparse channel estimation*, *Comm. Mag.*, **48**(11):164–174, 2010. 1
- [17] J. Bobin, J. Starck, and R. Ottensamer, *Compressed sensing in astronomy*, *J. Sel. Topics Signal Process.*, **2**(5):718–726, 2008. 1
- [18] S. Boccaletti, V. Latora, Y. Moreno, M. Chavez, and D.-U. Hwang, *Complex networks: Structure and dynamics*, *Phys. Rep.*, **424**:175–308, 2006. 1
- [19] A.M. Bruckstein, D.L. Donoho, and M. Elad, *From sparse solutions of systems of equations to sparse modeling of signals and images*, *SIAM Rev.*, **51**(1):34–81, 2009. 2.2
- [20] A.N. Burkitt, *A review of the integrate-and-fire neuron model: I. Homogeneous synaptic input*, *Biol. Cybern.*, **95**(2):97–112, 2006. 2.1
- [21] M. Cadenasso, S. Pickett, and J. Grove, *Dimensions of ecosystem complexity: Heterogeneity, connectivity, and history*, *Ecol. Complex.*, **3**(1):1–12, 2006. 1
- [22] D. Cai, A.V. Rangan, and D.W. McLaughlin, *Architectural and synaptic mechanisms underlying coherent spontaneous activity in V1*, *Proc. Natl. Acad. Sci. USA*, **102**:5868–5873, 2005. 2.1
- [23] D. Cai, L. Tao, M. Shelley, and D.W. McLaughlin, *An effective representation of fluctuation-driven neuronal networks with application to simple and complex cells in visual cortex*, *Proc. Natl. Acad. Sci. USA*, **101**:7757–7762, 2004. 2.3
- [24] E.J. Candes and M.B. Wakin, *An introduction to compressive sampling*, *Signal Process. Mag. IEEE*, **25**(2):21–30, 2008. 1, 2.2
- [25] E.J. Candes, J.K. Romberg, and T. Tao, *Stable signal recovery from incomplete and inaccurate measurements*, *Commun. Pure Appl. Math.*, **59**(8):1207–1223, 2006. 1, 2.2, 2.2, 3.2
- [26] R. Dahlhaus, M. Eichler, and J. Sandkuhler, *Identification of synaptic connections in neural ensembles by graphical models*, *J. Neurosci. Meth.*, **77**(1):93–107, 1997. 1
- [27] W. Dai, M.A. Sheikh, O. Milenkovic, and R.G. Baraniuk, *Compressive sensing DNA microarrays*, *J. Bioinform. Syst. Biol.*, **162824**, 2009. 1
- [28] D. di Bernardo, M.J. Thompson, T.S. Gardner, S.E. Chobot, E.L. Eastwood, A.P. Wojtovich, S.J. Elliott, S.E. Schaus, and J.J. Collins, *Chemogenomic profiling on a genome-wide scale using reverse-engineered gene networks*, *Nat. Biotechnol.*, **23**(3):377–383, 2005. 1
- [29] D.L. Donoho, *Compressed sensing*, *IEEE Trans. Inform. Theory*, **52**:1289–1306, 2006. 1, 2.2, 3.2
- [30] D.L. Donoho and Y. Tsaig, *Fast solution of  $l_1$ -norm minimization problems when the solution may be sparse*, *IEEE Trans. Inform. Theory*, **54**(11):4789–4812, 2008. 2.2
- [31] B. Drossel and A. McKane, *Modelling food webs*, in S. Bornholdt and H.G. Schuster (eds.), *Handbook of Graphs and Networks*, Wiley-VCH, Berlin, 08, 2002. 1
- [32] N. Eagle, A.S. Pentland, and D. Lazer, *Inferring friendship network structure by using mobile phone data*, *Proc. Natl. Acad. Sci. USA*, **106**(36):15274–15278, 2009. 1

- [33] S. Eldawlatly, Y. Zhou, R. Jin, and K.G. Oweiss, *On the use of dynamic Bayesian networks in reconstructing functional neuronal networks from spike train ensembles*, *Neural Comput.*, **22**(1):158–189, 2010. 1
- [34] D.D. Feng, K. Wong, C. Wu, and W. Siu, *A technique for extracting physiological parameters and the required input function simultaneously from pet image measurements: theory and simulation study*, *IEEE Trans. Inf. Technol. Biomed.*, **1**(4):243–254, 1997. 1
- [35] D.J. Field, *What is the goal of sensory coding?* *Neural Comput.*, **6**(4):559–601, 1994. 1
- [36] S. Ganguli and H. Sompolinsky, *Compressed sensing, sparsity, and dimensionality in neuronal information processing and data analysis*, *Annu. Rev. Neurosci.*, **35**:485–508, 2012. 4
- [37] E. Ganmor, R. Segev, and E. Schneidman, *Sparse low-order interaction network underlies a highly correlated and learnable neural population code*, *Proc. Natl. Acad. Sci. USA*, **108**(23):9679–9684, 2011. 1
- [38] E. Ganmor, R. Segev, and E. Schneidman, *The architecture of functional interaction networks in the retina*, *J. Neurosci.*, **31**(8):3044–3054, 2011. 1
- [39] T.S. Gardner, D. di Bernardo, D. Lorenz, and J.J. Collins, *Inferring genetic networks and identifying compound mode of action via expression profiling*, *Science*, **301**(5629):102–105, 2003. 1
- [40] M. Gomez-Rodriguez, J. Leskovec, and A. Krause, *Inferring networks of diffusion and influence*, *T. Knowl. Discov. D.*, **5**(4):21, 2012. 1
- [41] J.M. Goncalves and S. Warnick, *Necessary and sufficient conditions for dynamical structure reconstruction of LTI networks*, *IEEE Trans. Automat. Contr.*, **53**(7):1670–1674, 2008. 1
- [42] D. Gross, Y.K. Liu, S.T. Flammia, S. Becker, and J. Eisert, *Quantum state tomography via compressed sensing*, *Phys. Rev. Lett.*, **105**(15):150401, 2010. 1
- [43] Y. Hata, T. Tsumoto, H. Sato, and H. Tamura, *Horizontal interactions between visual cortical neurones studied by cross-correlation analysis in the cat*, *J. Physiol.*, **441**:593–614, 1991. 1
- [44] Y. He, Z.J. Chen, and A.C. Evans, *Small-world anatomical networks in the human brain revealed by cortical thickness from MRI*, *Cereb. Cortex*, **17**(10):2407–2419, 2007. 1
- [45] M.A. Herman and T. Strohmer, *High-resolution radar via compressed sensing*, *Trans. Sig. Proc.*, **57**(6):2275–2284, 2009. 1
- [46] L. Holley and M. Karplus, *Protein secondary structure prediction with a neural network*, *Proc. Natl. Acad. Sci. USA*, **86**(1):152–156, 1989. 4
- [47] L. Hufnagel, D. Brockmann, and T. Geisel, *Forecast and control of epidemics in a globalized world*, *Proc. Natl. Acad. Sci. USA*, **101**(42):15124–15129, 2004. 1
- [48] M.D. Humphries, K. Gurney, and T.J. Prescott, *The brainstem reticular formation is a small-world, not scale-free, network*, *Proc. Biol. Sci.*, **273**(1585):503–511, 2006. 4
- [49] G. Isley, C.J. Hillar, and F.T. Sommer, *Deciphering subsampled data: adaptive compressive sampling as a principle of brain communication*, in J.D. Lafferty, C.K.I. Williams, J. Shawe-Taylor, R.S. Zemel and A. Culotta (eds.), *Advances in Neural Information Processing Systems*, Curran Associates, Inc., 910–918, 2010. 4
- [50] Y. Iturria-Medina, R.C. Sotero, E.J. Canales-Rodriguez, Y. Aleman-Gomez, and L. Melie-Garcia, *Studying the human brain anatomical network via diffusion-weighted MRI and graph theory*, *Neuroimage*, **40**(3):1064–1076, 2008. 1
- [51] R.E. Kalman, *A new approach to linear filtering and prediction problems*, *J. Basic Eng.*, **82**(1):35–45, 1960. 1
- [52] N.Z. Kirkham, J.A. Slemmer, and S.P. Johnson, *Visual statistical learning in infancy: evidence for a domain general learning mechanism*, *Cognition*, **83**(2):35–42, 2002. 4
- [53] G. Laurent, *Dynamical representation of odors by oscillating and evolving neural assemblies*, *Trends Neurosci.*, **19**(11):489–496, 1996. 1
- [54] M. Lustig, D. Donoho, and J.M. Pauly, *Sparse MRI: The application of compressed sensing for rapid MR imaging*, *Magn. Reson. Med.*, **58**(6):1182–1195, 2007. 1
- [55] H. Lutcke, F. Gerhard, F. Zenke, W. Gerstner, and F. Helmchen, *Inference of neuronal network spike dynamics and topology from calcium imaging data*, *Front. Neural. Circuits*, **7**:201, 2013. 3.3
- [56] N.T. Markov, M. Ercsey-Ravasz, D.C. Van Essen, K. Knoblauch, Z. Toroczkai, and H. Kennedy, *Cortical high-density counterstream architectures*, *Science*, **342**(6158):1238406, 2013. 1
- [57] N.T. Markov, P. Misery, A. Falchier, C. Lamy, J. Vezoli, R. Quilodran, M.A. Gariel, P. Giroud, M. Ercsey-Ravasz, L.J. Pilaz, C. Huissoud, P. Barone, C. Dehay, Z. Toroczkai, D.C. Van Essen, H. Kennedy, and K. Knoblauch, *Weight consistency specifies regularities of macaque cortical networks*, *Cereb. Cortex*, **21**(6):1254–1272, 2011. 3.1
- [58] H. Markram, J. Lubke, M. Frotscher, A. Roth, and B. Sakmann, *Physiology and anatomy of synaptic connections between thick tufted pyramidal neurones in the developing rat neocortex*, *J. Physiol.*, **500**(2):409–440, 1997. 1

[59] A. Mason, A. Nicoll, and K. Stratford, *Synaptic transmission between individual pyramidal neurons of the rat visual cortex in vitro*, *J. Neurosci.*, **11**(1):72–84, 1991. 1

[60] M. Massimini, F. Ferrarelli, R. Huber, S.K. Esser, H. Singh, and G. Tononi, *Breakdown of cortical effective connectivity during sleep*, *Science*, **309**(5744):2228–2232, 2005. 4

[61] R.E. Mirollo and S.H. Strogatz, *Synchronization of pulse-coupled biological oscillators*, *SIAM J. Appl. Math.*, **50**(6):1645–1662, 1990. 2.1

[62] B.A. Olshausen and D.J. Field, *Natural image statistics and efficient coding*, *Network*, **7**(2):333–339, 1996. 4

[63] B.A. Olshausen and D.J. Field, *Sparse coding with an overcomplete basis set: a strategy employed by V1?*, *Vision Res.*, **37**(23):3311–3325, 1997. 4

[64] D.S. Peterka, H. Takahashi, and R. Yuste, *Imaging voltage in neurons*, *Neuron*, **69**(1):9–21, 2011. 3.3

[65] A.V. Rangan, D Cai, and D.W. McLaughlin, *Modeling the spatiotemporal cortical activity associated with the line-motion illusion in primary visual cortex*, *Proc. Natl. Acad. Sci. USA*, **102**(52):18793–18800, 2005. 2.1

[66] T. Serre, A. Oliva, and T. Poggio, *A feedforward architecture accounts for rapid categorization*, *Proc. Natl. Acad. Sci. USA*, **104**(15):6424–6429, 2007. 4

[67] C.E. Shannon, *Communication in the presence of noise*, *Proceedings of the IRE*, **37**(1):10–21, 1949. 1, 2.2, 2.2

[68] R.A. Silver, *Neuronal arithmetic*, *Nat. Rev. Neurosci.*, **11**(7):474–489, 2010. 4

[69] S. Sokol, *Measurement of infant visual acuity from pattern reversal evoked potentials*, *Vision Res.*, **18**(1):33–39, 1978. 4

[70] D. Somers, S. Nelson, and M. Sur, *An emergent model of orientation selectivity in cat visual cortical simple cells*, *J. Neuroscience*, **15**:5448–5465, 1995. 2.1

[71] S. Song, P.J. Sjostrom, M. Reigl, S. Nelson, and D.B. Chklovskii, *Highly nonrandom features of synaptic connectivity in local cortical circuits*, *PLoS Biol.*, **3**(3):e68, 2005. 1

[72] M.S. Spina, M.J. Schwartz, D.H. Staelin, and A.J. Gaisewski, *Application of multilayer feed-forward neural networks to precipitation cell-top altitude estimation*, *IEEE Trans. Geosci. Remote Sensing*, **36**(1):154–162, 1998. 4

[73] O. Sporns, *The human connectome: a complex network*, *Ann. N. Y. Acad. Sci.*, **1224**:109–125, 2011. 1

[74] I.H. Stevenson, J.M. Rebesco, L.E. Miller, and K.P. Kording, *Inferring functional connections between neurons*, *Curr. Opin. Neurobiol.*, **18**(6):582–588, 2008. 1

[75] S.H. Strogatz, *Exploring complex networks*, *Nature*, **410**:268–276, 2001. 1

[76] A. Treves, *Mean field analysis of neuronal spike dynamics*, *Network*, **4**:259–284, 1993. 2.3

[77] J.A. Tropp and A.C. Gilbert, *Signal recovery from random measurements via orthogonal matching pursuit*, *IEEE Trans. Inform. Theory*, **53**(12):4655–4666, 2007. 2.2

[78] L.R. Varshney, B.L. Chen, E. Paniagua, D.H. Hall, and D.B. Chklovskii, *Structural properties of the *Caenorhabditis elegans* neuronal network*, *PLoS Comput. Biol.*, **7**(2):e1001066, 2011. 1

[79] J.D. Victor, *Nonlinear systems analysis in vision: Overview of kernel methods*, in R.B. Pinter and B. Nabat (eds.), *Nonlinear Vision: Determination of Neural Receptive Fields, Function, and Networks*, CRC Press, Boca Raton, 1–37, 1992. 4

[80] D.J. Watts and S.H. Strogatz, *Collective dynamics of ‘small-world’ networks*, *Nature*, **393**(6684):440–442, 1998. 1

[81] J.G. White, E. Southgate, J.N. Thomson, and S. Brenner, *The structure of the nervous system of the nematode *Caenorhabditis elegans**, *Philos. Trans. R. Soc. Lond., B, Biol. Sci.*, **314**(1165):1–340, 1986. 1

[82] N. Wiener, *Nonlinear Problems in Random Theory*, The Technology Press of Massachusetts Institute of Technology, Cambridge, 1958. 4

[83] S.R. Williams and C. Wozny, *Errors in the measurement of voltage-activated ion channels in cell-attached patch-clamp recordings*, *Nat. Commun.*, **2**:242, 2011. 3.3

[84] D. Zhou, A.V. Rangan, D.W. McLaughlin, and D. Cai, *Spatiotemporal dynamics of neuronal population response in the primary visual cortex*, *Proc. Natl. Acad. Sci. USA*, **110**(23):9517–9522, 2013. 2.1

[85] D. Zhou, Y. Xiao, Y. Zhang, Z. Xu, and D. Cai, *Causal and structural connectivity of pulse-coupled nonlinear networks*, *Phys. Rev. Lett.*, **111**(5):054102, 2013. 1

[86] D. Zhou, Y. Xiao, Y. Zhang, Z. Xu, and D. Cai, *Granger causality network reconstruction of conductance-based integrate-and-fire neuronal systems*, *PLoS ONE*, **9**(2):e87636, 2014. 1